

We are IntechOpen, the world's leading publisher of Open Access books Built by scientists, for scientists

6,900

Open access books available

186,000

International authors and editors

200M

Downloads

Our authors are among the

154

Countries delivered to

TOP 1%

most cited scientists

12.2%

Contributors from top 500 universities



WEB OF SCIENCE™

Selection of our books indexed in the Book Citation Index
in Web of Science™ Core Collection (BKCI)

Interested in publishing with us?
Contact book.department@intechopen.com

Numbers displayed above are based on latest data collected.
For more information visit www.intechopen.com



Convergence Acceleration of Iterative Algorithms for Solving Navier–Stokes Equations on Structured Grids

Sergey Martynenko

Central Institute of Aviation Motors
Russia

1. Introduction

Basic tendency in computational fluid dynamics (CFD) consists in development of black box software for solving scientific and engineering problems. Numerical methods for solving nonlinear partial differential equations in black box manner should satisfy to the requirements:

- the least number of the problem-dependent components
- high computational efficiency
- high parallelism
- the least usage of the computer resources.

We continue with the 2D ($N = 2$) Navier–Stokes equations governing flow of a Newtonian, incompressible viscous fluid. Let $\Omega \in \mathbb{R}^N$ be a bounded, connected domain with a piecewise smooth boundary $\partial\Omega$. Given a boundary data, the problem is to find a nondimensional velocity field and nondimensional pressure such that:

- continuity equation

$$\frac{\partial u}{\partial x} + \frac{\partial v}{\partial y} = 0, \quad (1)$$

- X-momentum

$$\frac{\partial u}{\partial t} + \frac{\partial(u^2)}{\partial x} + \frac{\partial(vu)}{\partial y} = -\frac{\partial p}{\partial x} + \frac{1}{\text{Re}} \left(\frac{\partial^2 u}{\partial x^2} + \frac{\partial^2 u}{\partial y^2} \right), \quad (2)$$

- Y-momentum

$$\frac{\partial v}{\partial t} + \frac{\partial(uv)}{\partial x} + \frac{\partial(v^2)}{\partial y} = -\frac{\partial p}{\partial y} + \frac{1}{\text{Re}} \left(\frac{\partial^2 v}{\partial x^2} + \frac{\partial^2 v}{\partial y^2} \right). \quad (3)$$

Reynold number Re is defined as

$$\text{Re} = \frac{\rho u_s l_s}{\mu},$$

where ρ and μ are density and viscosity, respectively. Choice of the velocity scale u_s and geometric scale l_s depends on the given problem.

Equations (1)–(3) can be rewritten in the operator form

$$\begin{cases} \mathcal{N}(\vec{V}) + \nabla P = F \\ \nabla \vec{V} = G \end{cases} \quad (4)$$

where \mathcal{N} is nonlinear convection-diffusion operator, F and G are source terms, \vec{V} and P are velocity and pressure, respectively. It is assumed that the operator \mathcal{N} accounts boundary conditions. Note that 2D and 3D Navier–Stokes equations can be written as equation (4), where first and second equations abbreviate momentum and continuity equations. Linearized discrete Navier–Stokes equations can be written in the matrix form

$$\begin{pmatrix} A & B^T \\ B & 0 \end{pmatrix} \begin{pmatrix} \alpha \\ \beta \end{pmatrix} = \begin{pmatrix} f \\ g \end{pmatrix} \quad (5)$$

in which α and β represent the discrete velocity and discrete pressure, respectively. Here nonsymmetric A is a block diagonal matrix corresponding to the linearized discrete convection-diffusion operator \mathcal{N} . The rectangular matrix B^T represents the discrete gradient operator while B represents its adjoint, the divergence operator.

Large linear system of saddle point type (5) cannot be solved efficiently by standard methods of computational algebra. Due to their indefiniteness and poor spectral properties, such systems represent a significant challenge for solver developers Benzi et al. (2005).

Preconditioned Uzawa algorithm enjoys considerable popularity in computational fluid dynamics. The iterations for solving the saddle point system (5) are given by

$$\begin{cases} A\alpha^{(k+1)} = -B^T\beta^{(k)} + f \\ Q\beta^{(k+1)} = Q\beta^{(k)} + (B\alpha^{(k+1)} - g) \end{cases} \quad (6)$$

where the matrix Q is some preconditioner.

Preconditioned Uzawa algorithm (6) defines the following way for improvement of the solvers for the Navier–Stokes equations:

1) *development of numerical methods for solving the boundary value problems.*

Uzawa iterations require fast numerical inversion of the matrices A and Q . Now algebraic and geometric multigrid methods are often used for the given purpose Wesseling (1991). Multigrid methods give algorithms that solve sparse linear system of N unknowns with $O(N)$ computational complexity for large classes of problems. Variant of geometric multigrid methods with the problem-independent transfer operators for black box or/and parallel implementation is proposed in Martynenko (2006; 2010).

2) *development of preconditioning.*

Error vector in Uzawa iterations satisfies to the condition

$$\|\beta - \beta^{(k+1)}\| \leq \|I - Q^{-1}BA^{-1}B^T\| \cdot \|\beta - \beta^{(k)}\|,$$

where β is an exact solution. Choice of the preconditioner Q so

$$\|I - Q^{-1}BA^{-1}B^T\| \leq q < 1$$

guarantees geometric convergence rate of the Uzawa iterations

$$\|\beta - \beta^{(k+1)}\| \leq q^{k+1}\|\beta - \beta^{(0)}\|.$$

Unfortunately the preconditioner Q is strongly problem-dependent component of the Uzawa algorithm. Additional problem arises at formulation of the boundary conditions for Q . As a rule, the preconditioner has some relaxation parameters and determination of their optimal values is sufficiently difficult problem. Now construction of the preconditioner is subject of intensive study Benzi et al. (2005).

3) *development of new approaches for convergence acceleration* of iterative algorithms for solving saddle point problems.

The main obstacles to be overcome are execution time requirements and the generation of computational grids in complex three-dimensional domains Benzi et al. (2005). Recently convergence acceleration technique based on original pressure decomposition has been proposed for structured grids Martynenko (2009). The technique can be used in black box software. The chapter represents detailed description of the approach and its application for benchmark and applied problems.

2. Remarks on solvers for simplified Navier–Stokes equations

Limited characteristics of the first computers and absence of efficient numerical methods put difficulties for simulation of fluid flows based on the full Navier–Stokes equations. As a result, computational fluid dynamics started from simulation of the simplest flows described by the simplified Navier–Stokes equations.

As an example, we consider 2D laminar flow between parallel plates. Figure 1 represents geometry of the problem. Assuming that the pressure is not changed across the flow ($p'_y = 0$ in case of $L \gg 1$), full Navier–Stokes equations can be reduced to the simplified form:

a) X-momentum and mass conservation equations

$$\left\{ \begin{array}{l} \frac{\partial u}{\partial t} + \frac{\partial(u^2)}{\partial x} + \frac{\partial(vu)}{\partial y} = -\frac{\partial p}{\partial x} + \frac{1}{\text{Re}} \left(\frac{\partial^2 u}{\partial x^2} + \frac{\partial^2 u}{\partial y^2} \right) \\ \int_0^1 u(t, x, y) dy = \int_0^1 u(t, 0, y) dy \end{array} \right. , \quad (7)$$

b) continuity equation (1).

Since the mass conservation equation follows from the continuity equation (1), system (7) must be solved first. Solution of system (7) gives velocity components u and pressure p . After that the continuity equation (1) is used for determination of v . The computations are repeated until the convergent solution will be obtained.

Let us consider solution of system (7) in details. Assume that an uniform computational grid ($h = h_x = h_y$) is generated. Linearized finite-differenced equations with block unknowns

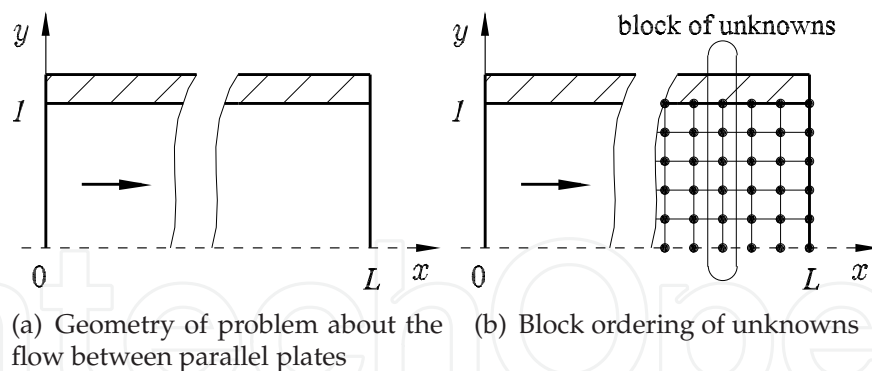


Fig. 1. Flow between parallel plates

ordering shown on Figure 1 are written as

$$\begin{cases} a_j u_{ij-1}^{(n+1)} + b_j u_{ij}^{(n+1)} + c_j u_{ij+1}^{(n+1)} = p_i^{(n+1)} + d_j \\ \sum_{j=1}^{N_y} u_{ij}^{(n+1)} = \frac{1}{h} G_0 \end{cases}, \quad (8)$$

where

$$G_0 = \int_0^1 u(t, 0, y) dy$$

is the given inlet mass flow rate and superscript n denotes time layer. Missing the superscript $(n+1)$, the system (8) can be rewritten in the matrix form

$$\begin{pmatrix} b_1 & c_1 & \cdots & 1 \\ a_2 & b_2 & c_2 & \cdots & 1 \\ & a_3 & b_3 & c_3 & \cdots & 1 \\ & & a_4 & b_4 & \cdots & 1 \\ \cdots & \cdots & \cdots & \cdots & \cdots & \cdots \\ 1 & 1 & 1 & 1 & \cdots & 0 \end{pmatrix} \begin{pmatrix} u_{i1} \\ u_{i2} \\ u_{i3} \\ u_{i4} \\ \cdots \\ p_i \end{pmatrix} = \begin{pmatrix} d_1 \\ d_2 \\ d_3 \\ d_4 \\ \cdots \\ h^{-1} G_0 \end{pmatrix}. \quad (9)$$

Comparison of systems (9) and (5) shows that solution of the simplified Navier–Stokes equations (7) also is reduced to solution of the saddle point system. The principal difference between systems (9) and (5) consists in size of zero block in the coefficient matrix. Since the zero block in system (9) has the least size 1×1 because of the pressure is independent on y , efficient iterative algorithms for solution of system (9) have been proposed and developed. The most promising of them is secant method Briley (1974), where error of the mass conservation equation

$$F(p_i^{(n+1)}) = \sum_{j=1}^{N_y} u_{ij}^{(n+1)}(p_i^{(n+1)}) - \frac{1}{h} G_0$$

is used for computation of pressure by the iterative method

$$p_i^{(k+1)} = p_i^{(k)} - \frac{p_i^{(k)} - p_i^{(k-1)}}{F_i^{(k)} - F_i^{(k-1)}} F_i^{(k)}, \quad k = 1, 2, \dots,$$

where superscript k denotes the secant method iterations. Note that the approach requires two starting guesses $p_i^{(0)}$ and $p_i^{(1)}$. First starting guess can be obtained by extrapolation. For example, for uniform grid we obtain $p_i^{(0)} = 2p_{i-1} - p_{i-2}$ and compute $F^{(0)}$. Second starting guess can be given by perturbation of the first one, for example $p_i^{(1)} = 1.001p_i^{(0)}$. It gives $F^{(1)}$. Function F depends almost linearly on $p_i^{(n+1)}$, but the secant method is direct solver for linear problems. Usually it is required several secant iterations to reduce error of the discrete mass conservation equation down to roundoff error.

Note that in 2D case the system (9) can be solved by direct methods, i.e. without the secant iterations. However in 3D case the direct methods require unpractical computational efforts due to five-diagonal structure of the coefficient matrix.

As contrasted to the Uzawa algorithm (6), the method does not require some preconditioner(s), relaxation parameter(s), extra computer memory and has high convergence rate. Unfortunately, basic assumption $p = p(t, x)$ does not allow apply the method directly for solving full Navier–Stokes equations (1)–(3). Accounting the attractive properties, the algorithm for solving the simplified Navier–Stokes equations can be used for convergence acceleration of the iterative methods intended for full Navier–Stokes equations.

Reduction of system (5) to the saddle point system with zero block of the least size is popular approach in CFD. For example, similar reduction based on special unknown ordering is used in Vanka smoother Vanka (1986).

3. Principle of formal decomposition of pressure

In order to apply the abovementioned approach for solving full Navier–Stokes equations, it is necessary artificially extract «one-dimensional parts of pressure» from the pressure field. For the given purpose, let add and subtract items $p^x(t, x)$, $p^y(t, y)$ and $p^z(t, z)$ depending only on one spatial variable, i.e.

$$p(t, x, y, z) = p^x(t, x) + p^y(t, y) + p^z(t, z) + \left(-p^x(t, x) - p^y(t, y) - p^z(t, z) + p(t, x, y, z) \right),$$

where superscripts x , y and z denote dependence of the functions on the spatial variables. Let us introduce a new function

$$p^{xyz}(t, x, y, z) = -p^x(t, x) - p^y(t, y) - p^z(t, z) + p(t, x, y, z).$$

Finally the pressure can be represented as

$$p(t, x, y, z) = p^x(t, x) + p^y(t, y) + p^z(t, z) + p^{xyz}(t, x, y, z). \quad (10)$$

Representation (10) will be called a principle of formal decomposition of pressure. *Basic idea of the method consists in application of the efficient numerical methods developed for the simplified Navier–Stokes equations for determination of part of pressure (i.e. for $p^x(t, x) + p^y(t, y) + p^z(t, z)$).* Fast computation of part of pressure results in reduction of total computational efforts needed for full Navier–Stokes equations.

In spite of simplicity of the representation (10), it is necessary to comment the principle of formal decomposition of pressure:

Remark 1. All items $p^x(t, x)$, $p^y(t, y)$, $p^z(t, z)$ and $p^{xyz}(t, x, y, z)$ have no physical meaning, but physical meaning has their sum. In follows, the items $p^x(t, x)$, $p^y(t, y)$ and $p^z(t, z)$ will be called as «one-dimensional components of the pressure», and $p^{xyz}(t, x, y, z)$ as «multidimensional component». The quotes «» will indicate absence of the physical meaning of the «pressure components».

Remark 2. In N -dimensional case ($N = 2, 3$) pressure is represented as sum of $N + 1$ «components», therefore the method requires N extra conditions for determination of the «one-dimensional components». The convergence acceleration technique uses N mass conservation equations as a priori information of physical nature.

Remark 3. In spite of representation of the pressure as sum of $N + 1$ «components», all momentum equations have only two «pressure» gradients. For example, for X -momentum we obtain

$$\begin{aligned}\frac{\partial p}{\partial x} &= \frac{\partial}{\partial x} \left(p^x(t, x) + p^y(t, y) + p^z(t, z) + p^{xyz}(t, x, y, z) \right) \\ &= \frac{\partial p^x}{\partial x} + \frac{\partial p^{xyz}}{\partial x}.\end{aligned}$$

Remark 4. Efficiency of the acceleration technique depends strongly on the flow nature. For directed fluid flows (for example, flows in nozzles, pipes etc.) gradient of one of «one-dimensional component of pressure» $p^x(t, x)$, $p^y(t, y)$ or $p^z(t, z)$ is dominant. In this case impressive reduction of computational work is expected as compared with traditional algorithms (i.e. $p^x(t, x) = p^y(t, y) = p^z(t, z) = 0$). However for rotated flows (for example, flow in a driven cavity) the approach shows the least efficiency.

Remark 5. In 3D case the method will be more efficient than in 2D case.

Remark 6. Velocity components and corresponding «one-dimensional components» in equation (10) are computed only in coupled manner. Velocity components and «multidimensional component» $p^{xyz}(t, x, y, z)$ in equation (10) can be computed in decoupled (segregated) or coupled manner.

Remark 7. Gradients of the «one-dimensional components» can be obtained in analytical form for explicit schemes. Implicit schemes require formulation of an auxiliary problem for determination of gradients of the «one-dimensional components».

4. Development of explicit schemes

First, consider modification of the explicit schemes using well-known benchmark problem about rotated flow in a driven cavity (Figure 2). Let a staggered grid with grid spacing h_x and h_y has been generated. Classical three-stage splitting scheme is represented as

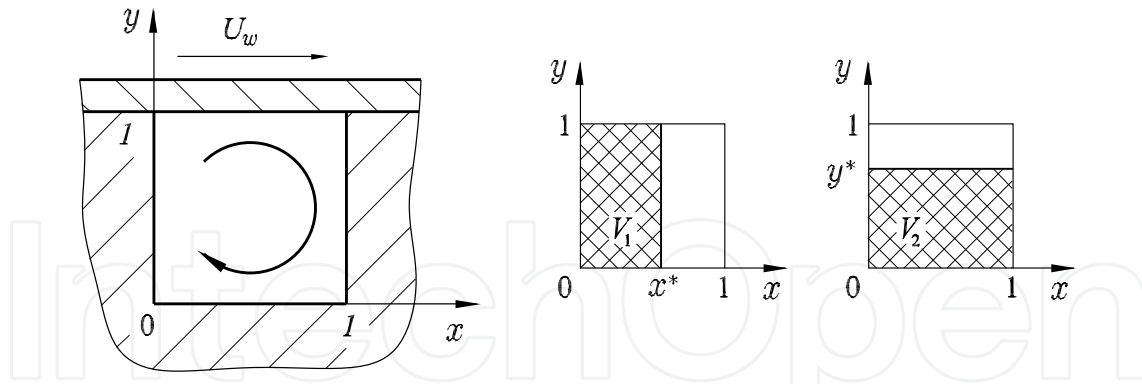


Fig. 2. Driven cavity and location of the control volumes V_1 and V_2

$$\begin{aligned} \text{Stage I:} \quad & \frac{V^{(n+1/2)} - V^{(n)}}{h_t} = -(V^{(n)} \nabla) V^{(n)} + \text{Re}^{-1} \Delta V^{(n)}, \\ \text{Stage II:} \quad & \Delta p = \frac{\nabla V^{(n+1/2)}}{h_t}, \\ \text{Stage III:} \quad & \frac{V^{(n+1)} - V^{(n+1/2)}}{h_t} = -\nabla p, \end{aligned}$$

where h_t is time semispacing, $V^{(n+1/2)}$ is intermediate velocity field and n is a time layer. Stage I consists in solution of the momentum equations without pressure gradients. For simplicity X-momentum can be written as

$$\frac{u_{ij}^{(n+1/2)} - u_{ij}^{(n)}}{h_t} = \psi_{ij}, \quad (11)$$

where ψ_{ij} is the given function defined as

$$\psi_{ij} = \left(-\frac{\partial(u^2)}{\partial x} - \frac{\partial(vu)}{\partial y} + \frac{1}{\text{Re}} \left(\frac{\partial^2 u}{\partial x^2} + \frac{\partial^2 u}{\partial y^2} \right) \right)_{ij}^{(n)}. \quad (12)$$

It is easy to see that intermediate velocity field $V^{(n+1/2)}$ is independent on pressure. This disadvantage can be compensated partially by the pressure decomposition (10). Application of the decomposition requires two mass conservation equations for 2D problems. Integration of the continuity equation (1) over the control volumes V_1 and V_2 shown on Figure 2 gives

$$\int_0^1 u(t, x, y) dy = 0, \quad \int_0^1 v(t, x, y) dx = 0. \quad (13)$$

Approximation of the mass conservation equations on the staggered grid is given by

$$h_y \sum_{j=1}^{N_y} u_{ij}^{(m)} = 0, \quad (14)$$

$$h_x \sum_{i=1}^{N_x} v_{ij}^{(m)} = 0, \quad (15)$$

where $m = n, n + 1/2, n + 1$ and $N_x = 1/h_x$, $N_y = 1/h_y$. As contrasted with equation (11) in the classical approach, the velocity component u and «one-dimensional component of pressure» p^x should satisfy to the system

$$\begin{cases} \frac{u_{ij}^{(n+1/2)} - u_{ij}^{(n)}}{h_t} = - \left(\frac{\partial p^x}{\partial x} \right)_i^{(n+1/2)} + \psi_{ij} \\ h_y \sum_{j=1}^{N_y} u_{ij}^{(n+1/2)} = 0 \end{cases}, \quad (16)$$

i.e. u and p^x are computed in the coupled manner using the discrete mass conservation equation (14).

It is clear that the system (16) can be written in form of (5), where A is the diagonal matrix for explicit schemes. This fact allows obtain analytic solution of the saddle point system (16). Multiplication of the first equation in system (16) on h_y and summation give

$$\frac{1}{h_t} \left(h_y \sum_{j=1}^{N_y} u_{ij}^{(n+1/2)} - h_y \sum_{j=1}^{N_y} u_{ij}^{(n)} \right) = - \sum_{j=1}^{N_y} h_y \left(\frac{\partial p^x}{\partial x} \right)_i^{(n+1/2)} + h_y \sum_{j=1}^{N_y} \psi_{ij}. \quad (17)$$

Left-hand side of the equation equals zero due to equation (14). Furthermore

$$\sum_{j=1}^{N_y} h_y \left(\frac{\partial p^x}{\partial x} \right)_i^{(n+1/2)} = \left(\frac{\partial p^x}{\partial x} \right)_i^{(n+1/2)} \sum_{j=1}^{N_y} h_y = \left(\frac{\partial p^x}{\partial x} \right)_i^{(n+1/2)},$$

because $(p^x)'_i$ is independent on j and $\sum_{j=1}^{N_y} h_y = 1$ is dimensionless height of the cavity.

Equation (17) is reduced to

$$\left(\frac{\partial p^x}{\partial x} \right)_i^{(n+1/2)} = h_y \sum_{j=1}^{N_y} \psi_{ij}. \quad (18)$$

Substitution of the equation into system (16) gives a new form of the system

$$\begin{cases} \frac{u_{ij}^{(n+1/2)} - u_{ij}^{(n)}}{h_t} = -h_y \sum_{j=1}^{N_y} \psi_{ij} + \psi_{ij} \\ \frac{(p^x)_i^{(n+1/2)} - (p^x)_{i-1}^{(n+1/2)}}{h_x} = h_y \sum_{j=1}^{N_y} \psi_{ij} \end{cases}, \quad (19)$$

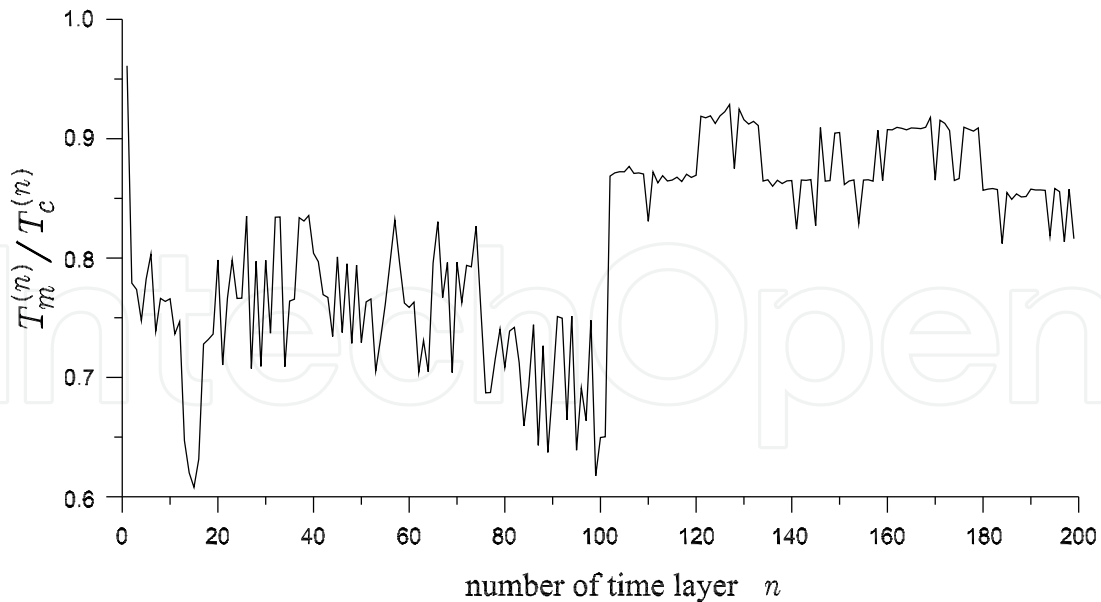


Fig. 3. Ratio of execution time at flow simulation in the driven cavity

where $(p^x)_0^{(n+1/2)}$ is some constant. It is clear that solution of system (19) is

$$u_{ij}^{(n+1/2)} = u_{ij}^{(n)} - h_t h_y \sum_{j=1}^{N_y} \psi_{ij} + h_t \psi_{ij},$$

$$(p^x)_i^{(n+1/2)} = (p^x)_{i-1}^{(n+1/2)} + h_x h_y \sum_{j=1}^{N_y} \psi_{ij}.$$

Velocity component u and «one-dimensional component of pressure» p^x are computed in the coupled manner saving explicit nature of the computation. Other velocity components are computed in the similar way.

Accounting decomposition (10), other stages of the algorithm are written as

$$\text{Stage II: } \Delta p^{xy} = \frac{\nabla V^{(n+1/2)}}{h_t},$$

$$\text{Stage III: } \frac{V^{(n+1)} - V^{(n+1/2)}}{h_t} = -\nabla p^{xy}.$$

In the stages only «multidimensional component» p^{xy} is used for computation of the velocity field.

For the numerical experiment law of the lid motion is taken as

$$U_w^{(n)} = \min \left(\frac{n}{100}; 1 \right).$$

Reynolds number $Re = 1000$ is based on the cavity height and the lid velocity $\max U_w^{(n)} = 1$. Staggered uniform grid $h_x = h_y = h = 1/200$, $h_t = h/5$ is used for the flow simulation. Ratio

of the execution time $T_m^{(n)}/T_c^{(n)}$ is used as a criterion of the convergence acceleration, where $T_m^{(n)}$ and $T_c^{(n)}$ are execution time for abovementioned and classical approaches, respectively. Figure 3 shows result of the numerical test. Obtained result for $n = 200$

$$\frac{1}{200} \sum_{n=1}^{200} T_m^{(n)}/T_c^{(n)} = 0.81$$

illustrate the least acceleration efficiency arising at simulation of the rotated flows.

5. Development of implicit schemes

Application of the pressure decomposition (10) for improvement of the implicit schemes requires solution of an auxiliary problem because of the «pressure» gradients can not be determined in explicit form such as equation (18).

5.1 Auxiliary problem

Auxiliary problem is intended for fast computation of the «one-dimensional components» $p^x(t, x)$, $p^y(t, y)$ and $p^z(t, z)$ in decomposition (10). It is assumed that the solution of the auxiliary problem will be close to the solution of the Navier–Stokes equations.

Formulation of the auxiliary problem is based on replacement of the continuity equation (1) by the mass conservation equations. For example, for the driven cavity (Figure 2) the auxiliary problem with the mass conservation equations (13) instead of the continuity equation (1) takes the form:

a) X-momentum and mass conservation equations

$$\left\{ \begin{array}{l} \frac{\partial u}{\partial t} + \frac{\partial(u^2)}{\partial x} + \frac{\partial(vu)}{\partial y} = -\frac{\partial p^x}{\partial x} - \left[\frac{\partial p^{xy}}{\partial x} \right] + \frac{1}{\text{Re}} \left(\frac{\partial^2 u}{\partial x^2} + \frac{\partial^2 u}{\partial y^2} \right) \\ \int_0^1 u(t, x, y) dy = 0 \end{array} \right. , \quad (20)$$

b) Y-momentum and mass conservation equations

$$\left\{ \begin{array}{l} \frac{\partial v}{\partial t} + \frac{\partial(uv)}{\partial x} + \frac{\partial(v^2)}{\partial y} = -\frac{\partial p^y}{\partial y} - \left[\frac{\partial p^{xy}}{\partial y} \right] + \frac{1}{\text{Re}} \left(\frac{\partial^2 v}{\partial x^2} + \frac{\partial^2 v}{\partial y^2} \right) \\ \int_0^1 v(t, x, y) dx = 0 \end{array} \right. , \quad (21)$$

where square brackets mean that the «pressure» gradients $(p^{xy})'_x$ and $(p^{xy})'_y$ are fixed (i.e. its values are taken from previous iteration). Braces mean that the momentum and mass conservation equations are solved only in coupled manner.

Since the systems (20) and (21) are similar to the simplified Navier–Stokes equations (7), the systems can be solved by the same numerical methods. Main difference consists in stopping criterion: auxiliary problem can be solved approximately, i.e. it is necessary to perform several iterations of line Seidel method with the secant iterations. As a result, extra computational

work for approximated solution of the auxiliary problem is negligible small as compared with the total efforts. Note that the equations of the auxiliary problem are not pressure-linked.

To illustrate influence of the auxiliary problem on convergence rate, we use Uzawa algorithm (6) for simulation of stationary flow in the driven cavity starting the iterand zero: $u^{(0)} = 0$, $v^{(0)} = 0$ and $p^{(0)} = 0$. Accounting zero boundary conditions for v , first equation of system (6) is reduced to

$$\frac{\partial(u^2)}{\partial x} = \frac{1}{\text{Re}} \left(\frac{\partial^2 u}{\partial x^2} + \frac{\partial^2 u}{\partial y^2} \right) \quad (22)$$

and $v = 0$. In the auxiliary problem the system (20) takes the form

$$\begin{cases} \frac{\partial(u^2)}{\partial x} = -\frac{dp^x}{dx} + \frac{1}{\text{Re}} \left(\frac{\partial^2 u}{\partial x^2} + \frac{\partial^2 u}{\partial y^2} \right) \\ \int_0^1 u(x,y) dy = 0 \end{cases} \quad (23)$$

and $v = 0$. Finally both problem (22) and (23) are reduced to systems of linear algebraic equations $Ax = b$. For clearness these equations are solved until

$$\frac{\|Ax - b\|}{\|b\|} < 10^{-7}.$$

The computations are performed with $\text{Re} = 100$ on uniform staggered grid 101×101 ($h_x = h_y = 1/100$).

Figure 4 represents solution of the Navier–Stokes equations in “stream function–vorticity” (+) Ghia et al. (1982), primitive variables formulations (—) and solutions of equations (22) and (23) in the middle section of the cavity ($x = 0.5$) at $\text{Re} = 100$. It is easy to see that use of the mass conservation equations in the auxiliary problem makes it possible to obtain more accurate approximation to solution of the full Navier–Stokes equations (1)–(3).

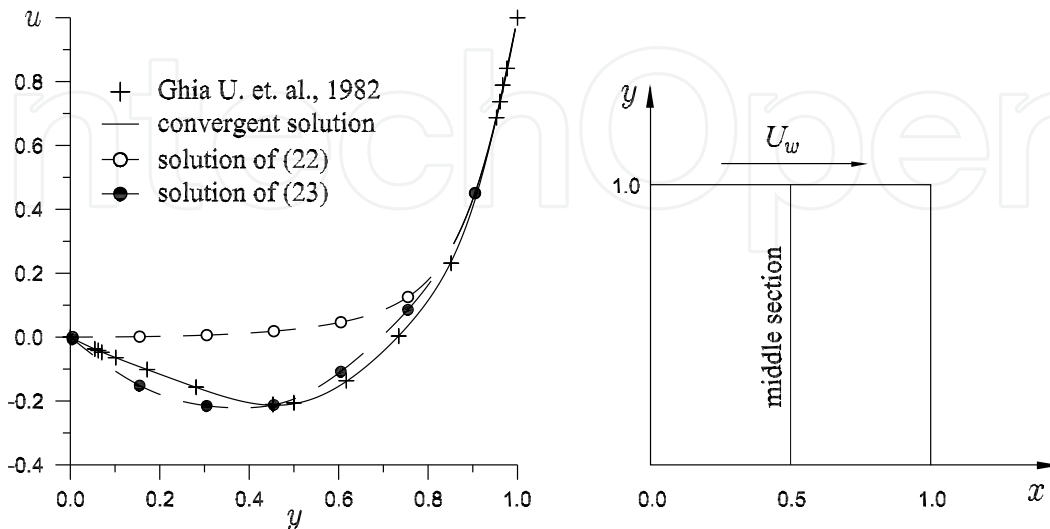


Fig. 4. Distribution of the velocity component u in the middle section of the cavity

5.2 Main problem

Accounting the pressure decomposition (10), the momentum equations in the main problem are written as

$$\frac{\partial u}{\partial t} + \frac{\partial(u^2)}{\partial x} + \frac{\partial(vu)}{\partial y} = - \left[\frac{dp^x}{dx} \right] - \frac{\partial p^{xy}}{\partial x} + \frac{1}{\text{Re}} \left(\frac{\partial^2 u}{\partial x^2} + \frac{\partial^2 u}{\partial y^2} \right), \quad (24)$$

$$\frac{\partial v}{\partial t} + \frac{\partial(uv)}{\partial x} + \frac{\partial(v^2)}{\partial y} = - \left[\frac{dp^y}{dy} \right] - \frac{\partial p^{xy}}{\partial y} + \frac{1}{\text{Re}} \left(\frac{\partial^2 v}{\partial x^2} + \frac{\partial^2 v}{\partial y^2} \right), \quad (25)$$

where square brackets mean that the «pressure» gradients $(p^x)'$ and $(p^y)'$ are fixed (i.e. the gradients have been computed in the auxiliary problem (such as equation (20) and (21) for the driven cavity)). Main problem consists of momentum (24), (25) and continuity equations (1). Algorithm for simulation of the flows with given mass flow rate can be represented as:

Stage I: *auxiliary problem*: several iterations of line (2D) or plane (3D) Seidel method with the secant iterations

Stage II: *main problem*: iterations of basic method (SIMPLE, Uzawa or Vanka iterations, etc.)

Stage III: check convergence, continue (go to 1) if necessary

5.3 Flow over a backward-facing step

The next benchmark problem about backward-facing step flow is used for illustration of the impressive convergence acceleration for the directed fluid flows.

Consider the stationary laminar flow over a backward-facing step, which is another well studied test case. Figure 5 shows the geometry of the flow. The fact that the solution of the incompressible Navier–Stokes equations over a backward-facing step at $\text{Re} = 800$ is steady and stable has been confirmed in a number of recent works.

No-slip boundary conditions are imposed on the step and the upper and lower walls, a parabolic velocity u profile is specified at the channel inlet ($v = 0$), and zero natural boundary conditions ($v = 0$ and $u'_x = 0$) are imposed at the channel outlet. The Reynolds number Re is based on the channel height ($H = 1$) and the average inlet velocity in the parabolic profile. The channel length is $L = 14$.

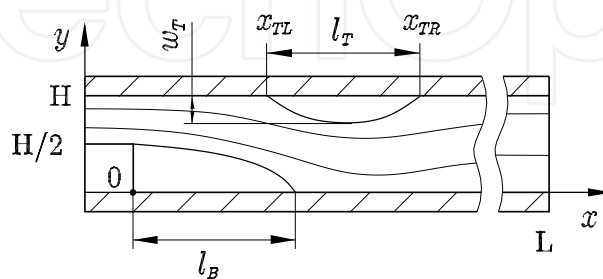


Fig. 5. Geometry of problem about the backward-facing step flow

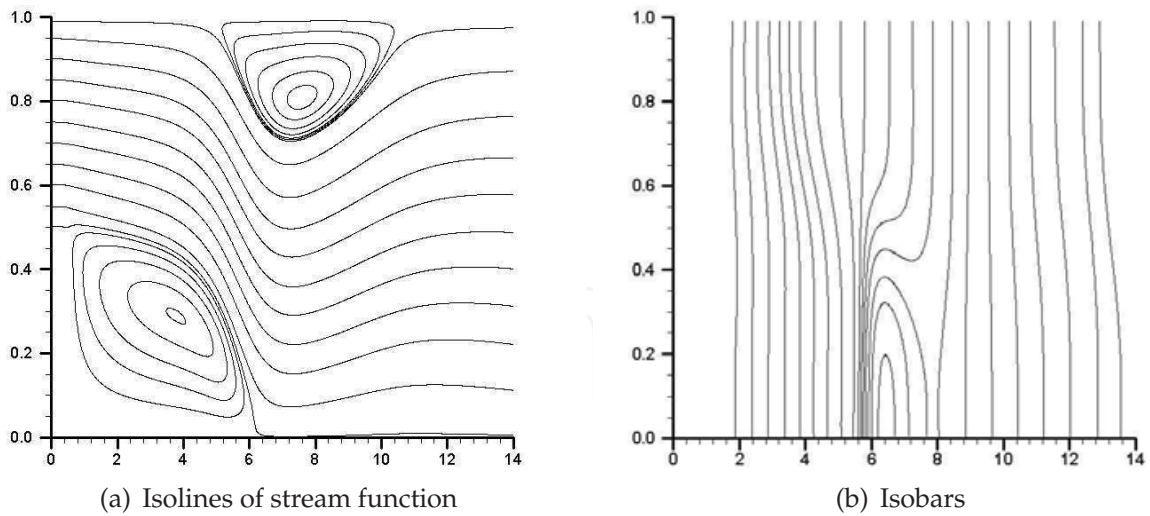


Fig. 6. Stationary flow over a backward-facing step

Redefining velocity components to be zero inside the step, we obtain the following mass conservation equations for the given problem

$$\int_0^H u(t, x, y) dy = \int_0^H u(t, 0, y) dy,$$

$$\int_0^L v(t, x, y) dx = - \int_0^y (u(t, L, \xi) - u(t, 0, \xi)) d\xi.$$

Numerical experiments show that execution time can be reduced in ~ 400 times for the given problem (staggered grid 101×1401 , unpreconditioned Uzawa algorithm, $Re = 800$). Figure 6 explains the impressive reduction of the computational efforts. It is easy to see that pressure is changed mainly in x direction except small subdomain near attachment point of bottom eddy (i.e. $p(x, y) \approx p^x(x)$). Since the «one-dimensional component of the pressure» $p^x(x)$ is computed in the auxiliary problem, the proposed algorithm is very efficient for solving the problem.

Table 1 represents comparison of obtained results.

Authors	l_B	l_T	w_T	x_{TL}	x_{TR}	Nodes
Barton (1997)	6.0150	5.6600	–	4.8200	10.4800	
Gartling (1990)	6.1000	5.6300	–	4.8500	10.4800	129681
Gresho et al. (1993)	6.0820	5.6260	–	4.8388	10.4648	245760
Gresho et al. (1993)	6.1000	5.6300	–	4.8600	10.4900	≥ 8000
Keskar & Lin (1999)	6.0964	5.6251	–	4.8534	10.4785	3737
present	6.1000	5.6300	0.28	4.8400	10.4700	141501

Table 1. Comparison of results of the flow simulation over backward-facing step ($Re = 800$)

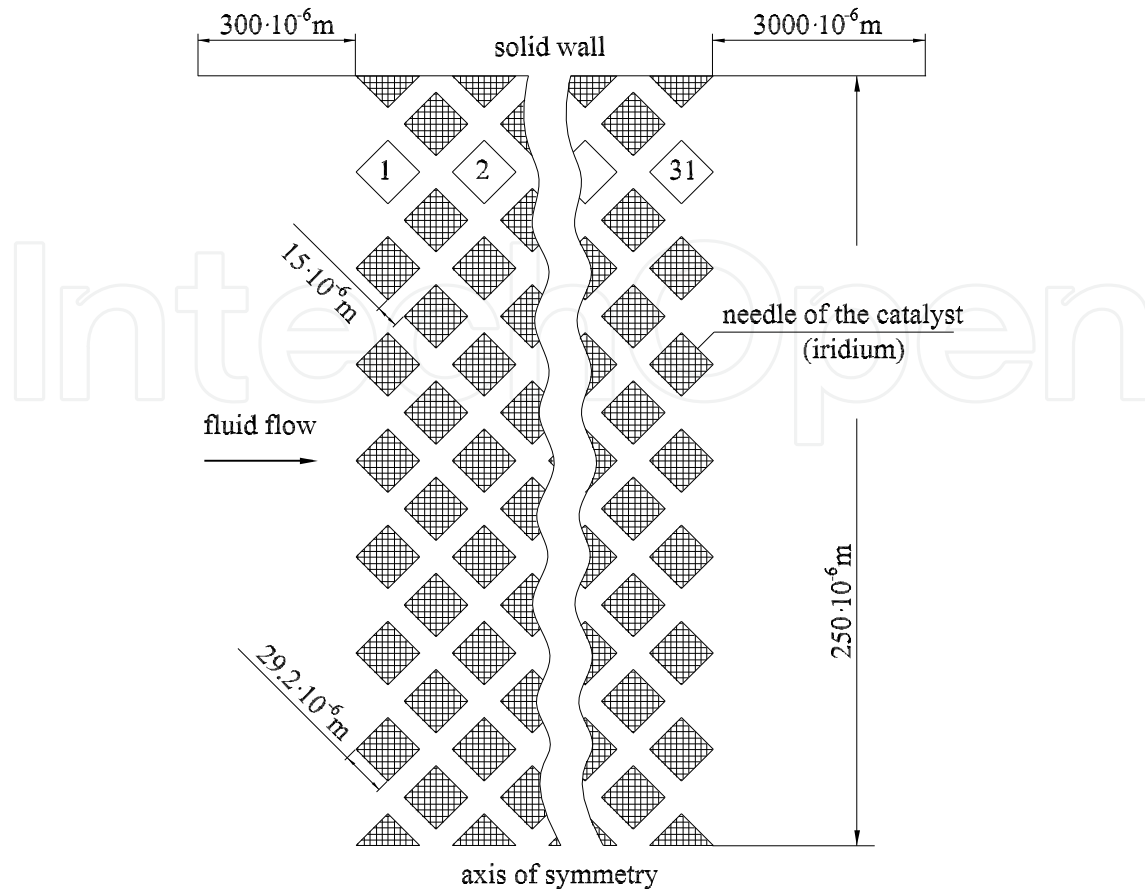


Fig. 7. Geometry of the microcatalyst

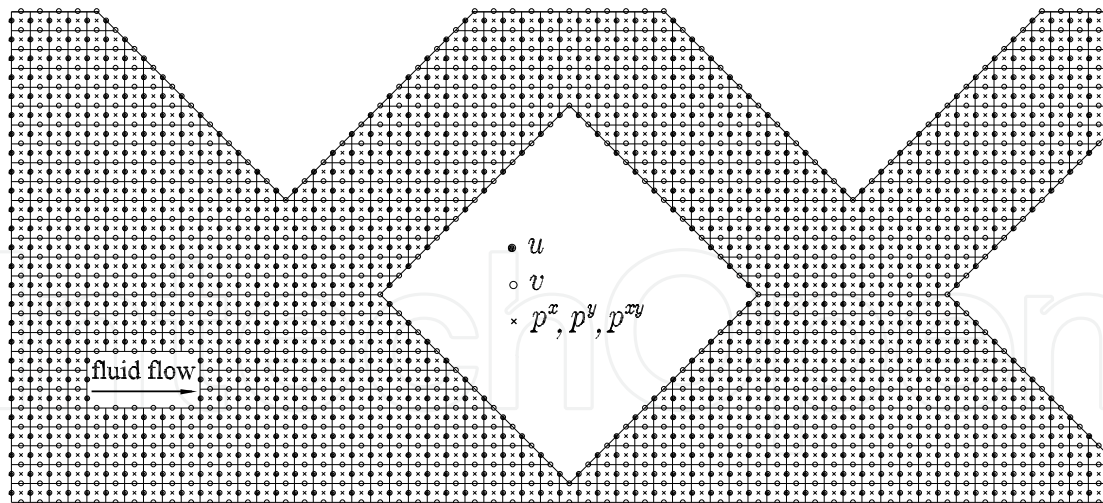


Fig. 8. Staggered grid in the microcatalyst

5.4 Flow in microcatalyst

Proposed approach has been used for simulation of incompressible fluid flows in microcatalyst. The microcatalyst represents 2D channel with iridium-covered needles located in chess order as shown on Figure 7.

Redefining velocity components to be zero inside the needles, there is no remarkable difference in formulation of the auxiliary problem for flow over backward-facing step and for

flow in the catalyst. Diffusion-dominant nature of fluid flow in the microcatalyst simplifies the grid generation. Example of the simplest computational grid for this problem is shown on Figure 8. No-slip conditions are approximated exactly on the needle surfaces.

Nonuniform staggered grid 385×3150 is used for the flow simulation ($Re = 350$). Figure 9 represents distribution of the stream function and pressure near first column of the needles. Chess order of the needle location results in eddy-free flow inside the microcatalyst. However intensive eddy formation after last column of the needles is observed (Figure 10).

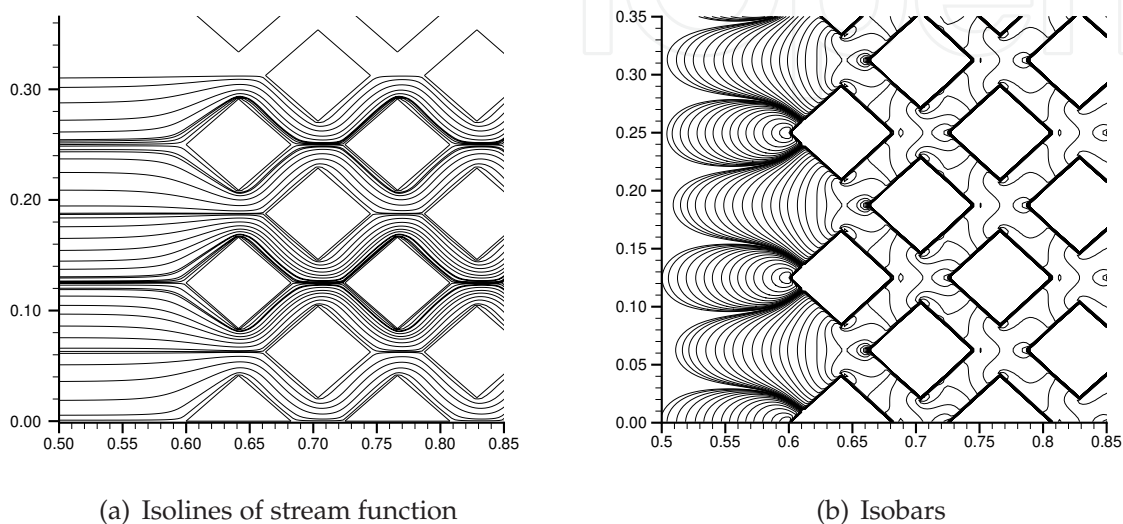


Fig. 9. Flow near first column of the needles

5.5 Compressible flow in laval micronozzle

Recently the numerical methods for fluid flow prediction have been classified into two categories: density-based and pressure-based. For the pressure-based approach, methods are

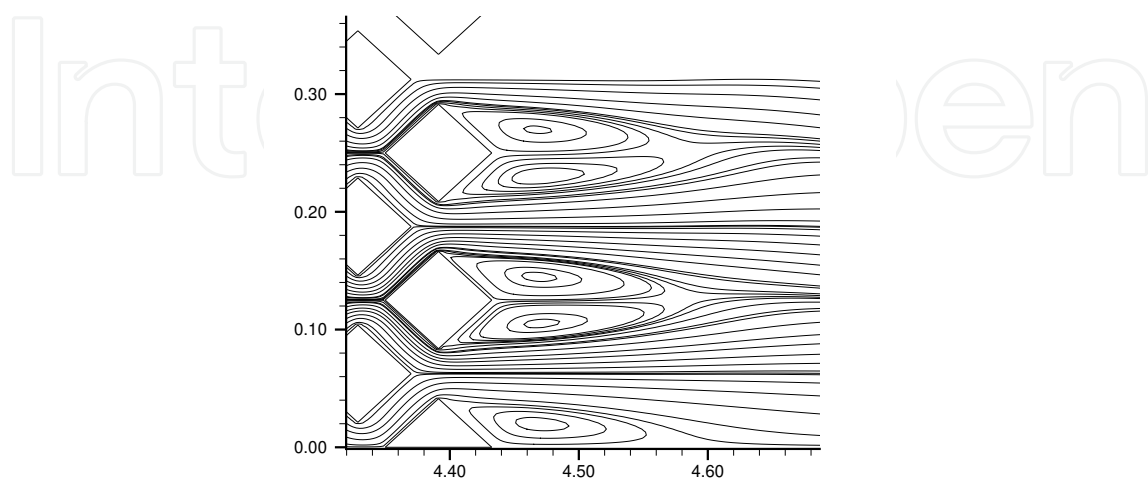


Fig. 10. Eddy formation after last column of the needles

classified into coupled and segregated (decoupled). Density-based algorithms traditionally are used to compute high speed compressible flows. Computational methods for low Mach number compressible flows are an active research field in recent years. The pressure-velocity coupling problem discussed earlier for incompressible flows are also encountered in the methods when used for low-speed applications.

Pressure decomposition (10) shows that there are not pure density-based and segregated solvers because of the velocity components and corresponding «one-dimensional components of pressure» (i.e. (u, p^x) , (v, p^y) and (w, p^z)) always are computed in the coupled manner. «Multidimensional component» p^{xyz} in (10) can be computed by coupled or segregated method using density-based or pressure-based approach.

Consider application of the pressure decomposition for simulation of compressible flow in flat Laval micronozzle. Width of subsonic part of the micronozzle is 1 mm. Grid generation is based on mapping of the non-dimensional physical domain with nonuniform grid onto computational domain (unit square) with uniform grid. Direct ($ABCD \rightarrow \bar{A}\bar{B}\bar{C}\bar{D}$) and reverse ($ABCD \leftarrow \bar{A}\bar{B}\bar{C}\bar{D}$) mappings are shown on Figure 11, where the function $\varphi(x)$ describes the micronozzle profile. The mappings can be given by

$$\bar{x} = x, \quad \bar{y} = -\frac{1}{\beta} \ln\left(1 - (1 - e^{-\beta})\frac{y}{\varphi(x)}\right),$$

where (x, y) and (\bar{x}, \bar{y}) are spatial variables in physical and computational domains, respectively. Parameter $\beta > 0$ is intended for the grid refinement near solid wall.

Jacobian (J) of the mapping

$$J = \begin{vmatrix} \bar{x}_x & \bar{x}_y \\ \bar{y}_x & \bar{y}_y \end{vmatrix} = \frac{1 - e^{-\beta}}{\beta} \frac{e^{\beta\bar{y}}}{\varphi(\bar{x})}$$

is non-singular ($J \neq 0$). In addition, $J \rightarrow 1/\varphi(\bar{x})$ at $\beta \rightarrow 0$ for uniform grid in y direction.

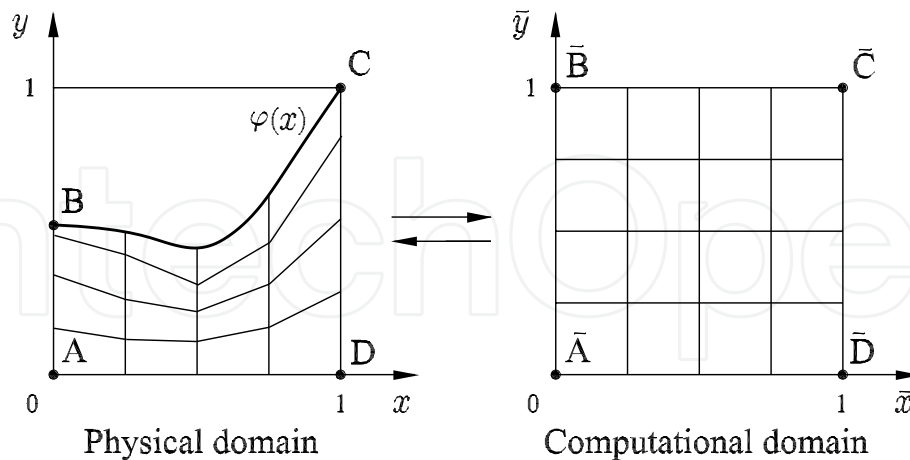


Fig. 11. Non-dimensional physical and computational domains

Finally, non-dimensional compressible Navier–Stokes equations in the computational domain are written as

$$\frac{\partial}{\partial t} \left(\frac{\mathbf{U}}{J} \right) + \epsilon \frac{\partial}{\partial \bar{x}} \left(\frac{\mathbf{E}}{J} \right) + \epsilon \frac{\partial}{\partial \bar{y}} \left(\frac{\bar{y}_x \mathbf{E}}{J} \right) + \frac{\partial \mathbf{F}}{\partial \bar{y}} = \frac{\mathbf{H}}{J},$$

where

$$\mathbf{U} = \begin{pmatrix} \rho \\ \rho u \\ \rho v \\ \rho i \end{pmatrix}, \quad \mathbf{H} = \begin{pmatrix} 0 \\ 0 \\ 0 \\ S \end{pmatrix},$$

$$\mathbf{E} = \begin{pmatrix} \rho u \\ \rho u^2 + p - \frac{4}{3} \frac{\epsilon}{\text{Re}} \left(\frac{\partial u}{\partial \bar{x}} + \bar{y}_x \frac{\partial u}{\partial \bar{y}} \right) + \frac{2}{3} \frac{\bar{y}_y}{\text{Re}} \frac{\partial v}{\partial \bar{y}} \\ \rho uv - \frac{\bar{y}_y}{\text{Re}} \frac{\partial v}{\partial \bar{y}} - \frac{\epsilon}{\text{Re}} \left(\frac{\partial v}{\partial \bar{x}} + \bar{y}_x \frac{\partial v}{\partial \bar{y}} \right) \\ \rho ui - \frac{\epsilon}{\text{Pe}} \left(\frac{\partial T}{\partial \bar{x}} + \bar{y}_x \frac{\partial T}{\partial \bar{y}} \right) \end{pmatrix},$$

$$\mathbf{F} = \begin{pmatrix} \rho v \\ \rho vu - \frac{\bar{y}_y}{\text{Re}} \frac{\partial u}{\partial \bar{y}} - \frac{\epsilon}{\text{Re}} \left(\frac{\partial v}{\partial \bar{x}} + \bar{y}_x \frac{\partial v}{\partial \bar{y}} \right) \\ \rho v^2 + p - \frac{4}{3} \frac{\bar{y}_y}{\text{Re}} \frac{\partial v}{\partial \bar{y}} + \frac{2}{3} \frac{\epsilon}{\text{Re}} \left(\frac{\partial u}{\partial \bar{x}} + \bar{y}_x \frac{\partial u}{\partial \bar{y}} \right) \\ \rho vi - \frac{\bar{y}_y}{\text{Pe}} \frac{\partial T}{\partial \bar{y}} \end{pmatrix}.$$

Parameter ϵ is the micronozzle width-to-length ratio.

First mass conservation equation is obtained by integration of the continuity equation as follows

$$\frac{\partial}{\partial t} \int_0^1 \int_0^x \frac{\rho(t, \xi, y)}{J} d\xi dy + \epsilon \int_0^1 \left(\frac{\rho u}{J} \right) \Big|_x dy - \epsilon \int_0^1 \left(\frac{\rho u}{J} \right) \Big|_0 dy = 0.$$

In the auxiliary problem for incompressible flows, iterations of line (2D) or plane (3D) Seidel method are stopped then the velocity component satisfies to the mass conservation equation. Computation of compressible flows requires updating of thermophysical properties (density ρ , coefficient of viscosity in Re and heat conductivity coefficient in Pe) using updated pressure in the line or plane. In 3D case values of thermophysical properties of the fluid for X-momentum should be updated using pressure

$$p(t, x, y, z) = p^x(t, x) + [p^y(t, y) + p^z(t, z) + p^{xyz}(t, x, y, z)],$$

temperature T and equation of state. Here square brackets mean that the pressure components p^y , p^z and p^{xyz} are fixed.

Figure 12 represents isobars in the Laval micronozzles. It is easy to see that the isobars are almost vertical lines near throat and in supersonic part of the micronozzle. It means that the pressure is changed mainly along the micronozzle axis. In other words, «one-dimensional component of the pressure» p^x in decomposition (10) is dominant in this problem. For

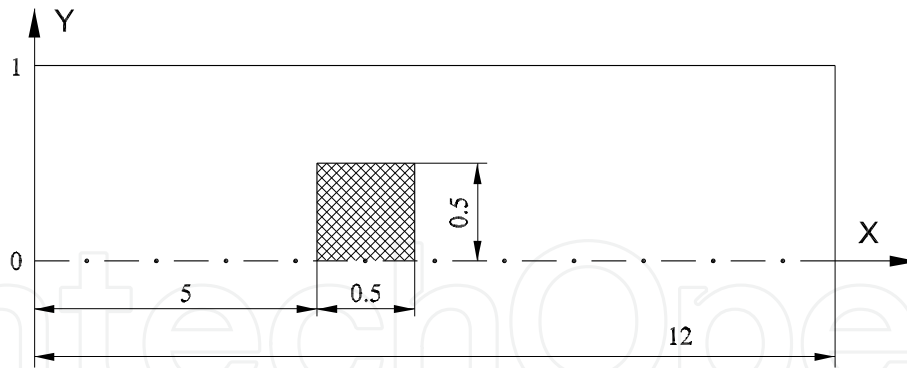


Fig. 13. Starting location of the plunger

the given problem, the auxiliary problem makes it possible to compute the most «part of pressure» (i.e. $p^x(t, x) + p^y(t, y)$) and corresponding change of thermophysical properties of the fluid based on simplified (pressure-unlinked) momentum equations in primitive variables formulation and mass conservation equations.

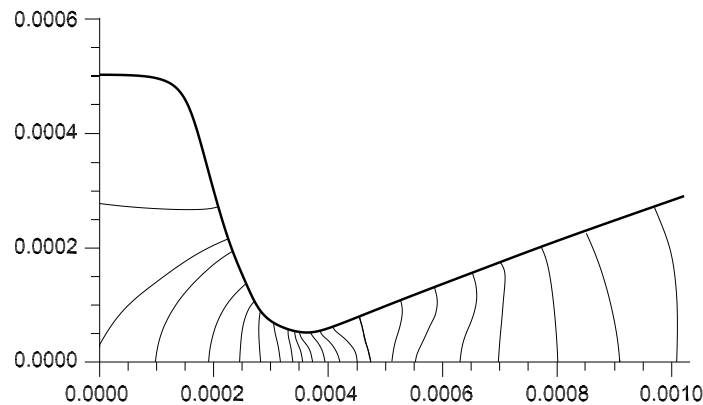


Fig. 12. Isobars in Laval micronozzle (sizes in meters)

5.6 Flows with unspecified mass rate

Previously fluid flows with the given mass rate have been simulated and analyzed. In some applications mass flow rate cannot be given in advance. The simplest example of such flows is problem about moving plunger. Immovable plunger is located between parallel plates filled by incompressible fluid. Figure 13 shows geometry of the problem and starting location of the plunger. Motion of the plunger causes the fluid flow. It is clear that mass flow rate depends on the plunger speed. Algorithm for simulation of the flows with unspecified mass rate should be modified as:

Stage I: *main problem*: iterations of basic method (SIMPLE, Uzawa or Vanka iterations, etc.)

Stage II: check convergence; continue if necessary

Stage III: *auxiliary problem*: several iterations of line (2D) or plane (3D) Seidel method with the secant iterations; continue (go to 1)

Assume that \tilde{u}_{ij} , \tilde{v}_{ij} and \tilde{p}_{ij}^{xy} are approximation to the solution of the Navier–Stokes equations obtained after iterations of the basic method. Then the mass conservation equation can be

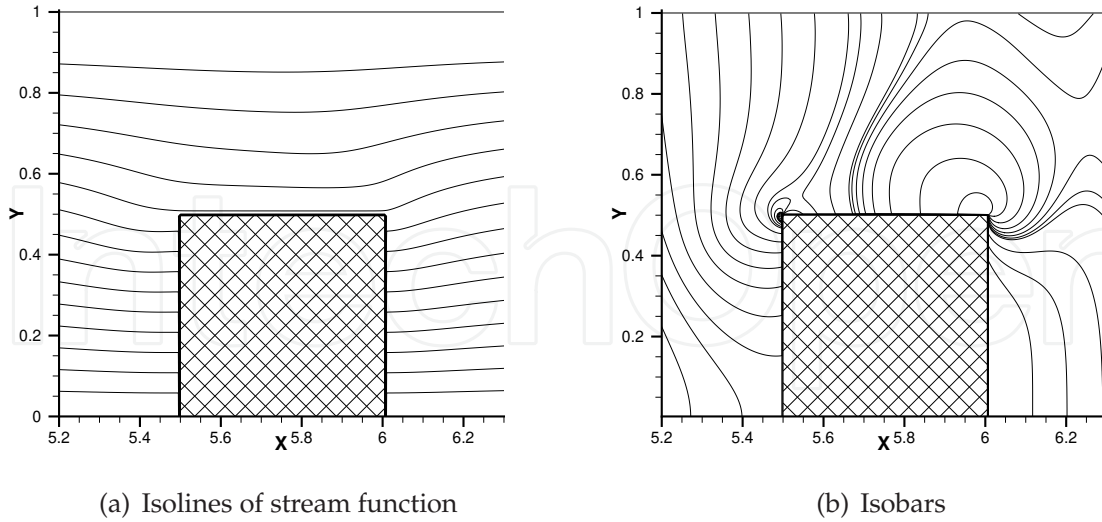


Fig. 14. Flow near the moving plunger

formulated as

$$\int_0^1 u(t, x_i, y) dy = \max_i \int_0^1 \tilde{u}(t, x_i, y) dy$$

at accelerated or uniform plunger motion and in form

$$\int_0^1 u(t, x_i, y) dy = \min_i \int_0^1 \tilde{u}(t, x_i, y) dy$$

at decelerated plunger motion. As a result, the auxiliary problem ensures expansion of perturbations caused by the plunger on all domain in each iteration. Uniform staggered grid 201×2401 ($h_x = h_y = 1/200$) is used for simulation the fluid flow around the moving plunger. Reynolds number $Re = 200$ is based on the plunger velocity and distance between the plates. Stream function isolines and isobars near the moving plunger are shown on Figure 14.

6. Pressure decomposition in geometric multigrid methods

Proposed convergence acceleration technique based on the pressure decomposition (10) should be incorporated with well-known algorithms for solving Navier–Stokes equations. Multigrid methods having (almost) optimal convergence rate for many applications seem to be the most promising solvers for many CFD problems. Our purpose is development of multigrid method with the least number of problem-dependent components for using in black box software.

6.1 Nonlinear multigrid iterations

To overcome problem of robustness, the Navier–Stokes equations (4) should be adapted for the multigrid algorithm Martynenko (2006). Adaptation of the Navier–Stokes equations (so called Σ -modification) consists in representation of the velocity \vec{V} and pressure P as sum of

two functions

$$\vec{V} = C_{\vec{V}} + \vec{V}, \quad P = C_P + \hat{P},$$

where discrete analogues of the functions $C_{\vec{V}}$ and C_P will be coarse grid corrections and discrete analogues of the functions \vec{V} and \hat{P} will be approximations to the solutions in the following multigrid iterations.

As a result, the Navier–Stokes equations (4) can be rewritten in the Σ -modified form

$$\begin{cases} \mathcal{N}(C_{\vec{V}} + \vec{V}) + \nabla(C_P + \hat{P}) = F \\ \nabla(C_{\vec{V}} + \vec{V}) = G \end{cases}.$$

Since $\mathcal{N}(C_{\vec{V}} + \vec{V}) = \mathcal{N}^*(C_{\vec{V}}) + \mathcal{N}(\vec{V})$, where $\mathcal{N}^* \neq \mathcal{N}$ for the nonlinear operator \mathcal{N} , we obtain

$$\begin{cases} \mathcal{N}^*(C_{\vec{V}}) + \nabla C_P = F^* \\ \nabla C_{\vec{V}} = G^* \end{cases}, \quad (26)$$

where $F^* = F - \mathcal{N}(\vec{V}) - \nabla \hat{P}$ and $G^* = G - \nabla \vec{V}$.

It is clear that main difference between Σ -modified and initial forms of the Navier–Stokes equations consists of the nonlinear convection-diffusion operator (\mathcal{N}^* in equation (26) instead of \mathcal{N} in equation (4)) and source terms (F^* and G^* in equation (26) instead of F and G in equation (4)). Note that Σ -modification does not require some linearization of the Navier–Stokes equations. Therefore modified Navier–Stokes equations with other transport equations can be solved in coupled manner on all coarse grids.

For example, 2D Σ -modified Navier–Stokes equations are written as:

a) Σ -modified continuity equation

$$\frac{\partial c^u}{\partial x} + \frac{\partial c^v}{\partial y} = R^{uv}(t, x, y),$$

b) Σ -modified X-momentum

$$\begin{aligned} \frac{\partial c^u}{\partial t} + \frac{\partial (c^u)^2}{\partial x} + 2 \frac{\partial (\hat{u}c^u)}{\partial x} + \frac{\partial (\hat{u}c^v)}{\partial y} + \frac{\partial (\hat{v}c^u)}{\partial y} + \frac{\partial (c^u c^v)}{\partial y} = \\ = -\frac{\partial c^p}{\partial x} + \frac{1}{\text{Re}} \left(\frac{\partial^2 c^u}{\partial x^2} + \frac{\partial^2 c^u}{\partial y^2} \right) + R^u(t, x, y), \end{aligned}$$

c) Σ -modified Y-momentum

$$\begin{aligned} \frac{\partial c^v}{\partial t} + \frac{\partial (\hat{u}c^v)}{\partial x} + \frac{\partial (\hat{v}c^u)}{\partial x} + \frac{\partial (c^u c^v)}{\partial x} + \frac{\partial (c^v)^2}{\partial y} + 2 \frac{\partial (\hat{v}c^v)}{\partial y} = \\ = -\frac{\partial c^p}{\partial y} + \frac{1}{\text{Re}} \left(\frac{\partial^2 c^v}{\partial x^2} + \frac{\partial^2 c^v}{\partial y^2} \right) + R^v(t, x, y), \end{aligned}$$

where discrete analogues of the functions c^u , c^v and c^p will be coarse grid corrections and discrete analogues of the functions \hat{u} , \hat{v} and \hat{p} will be approximations to the solutions in the following multigrid iterations. Source terms in the Σ -modified equations coincide with the

initial Navier–Stokes equations, i.e.

$$R^{uv}(t, x, y) = -\frac{\partial \hat{u}}{\partial x} - \frac{\partial \hat{v}}{\partial y},$$

$$R^u(t, x, y) = -\frac{\partial \hat{u}}{\partial t} - \frac{\partial(\hat{u}^2)}{\partial x} - \frac{\partial(\hat{v}\hat{u})}{\partial y} - \frac{\partial \hat{p}}{\partial x} + \frac{1}{\text{Re}} \left(\frac{\partial^2 \hat{u}}{\partial x^2} + \frac{\partial^2 \hat{u}}{\partial y^2} \right),$$

$$R^v(t, x, y) = -\frac{\partial \hat{v}}{\partial t} - \frac{\partial(\hat{u}\hat{v})}{\partial x} - \frac{\partial(\hat{v}^2)}{\partial y} - \frac{\partial \hat{p}}{\partial y} + \frac{1}{\text{Re}} \left(\frac{\partial^2 \hat{v}}{\partial x^2} + \frac{\partial^2 \hat{v}}{\partial y^2} \right),$$

Additional convection terms in Σ -modified momentum equations are result of nonlinear nature of the convection-diffusion operator \mathcal{N} , i.e. $\mathcal{N}^* \neq \mathcal{N}$. Approximation of the source terms R^{uv} , R^u and R^v defines the accuracy, monotonicity and conservatism of the numerical solutions. Approximation of other terms in the modified equations defines only multigrid convergence rate because $c^u \rightarrow 0$, $c^v \rightarrow 0$ and $c^p \rightarrow 0$ for convergent solution.

6.2 Multigrid structure

Recently variant of the geometric multigrid methods with the problem-independent transfer operators (so-called Robust Multigrid Technique) has been proposed and developed Martynenko (2006; 2010). The problem-independent restriction and prolongation operators are result of the multiple coarse grid corrections on subgrids of the finest grid.

Assume that a finest staggered grid G_1^0 has been generated in the domain. Coarsening in Robust Multigrid Technique is based on representation of the finest grid G_1^0 as union of 3^N ($N = 1, 2, 3$) coarse grids $G_1^1, G_2^1, \dots, G_{3^N}^1$ with the following properties:

1. all coarse grids $G_1^1, G_2^1, \dots, G_{3^N}^1$ have no common points, i.e. $G_n^1 \cap G_m^1 = \emptyset$, $n \neq m$.
2. the finest grid G_1^0 is the union of all coarse grids $G_1^1, G_2^1, \dots, G_{3^N}^1$, i.e. $G_1^0 = \bigcup_{k=1}^{3^N} G_k^1$.
3. all grids are similar to each other, but a mesh size on the coarse grids is three times as large as than the mesh size on the finest grid.
4. control volume on the coarse grids $G_1^1, G_2^1, \dots, G_{3^N}^1$ is union of 3^N control volumes on the finest grid G_1^0 .

The coarse grid generation is further recurrently repeated: each grid $G_1^1, G_2^1, \dots, G_{3^N}^1$ gives 3^N coarser grids. The coarse grid generation is finished when no further coarsening can be performed. Finally we obtain G_k^l , $l = 0, 1, \dots, L^+$, $k = 1, 3^{Nl}$ computational grids (so called a multigrid structure), where L^+ is number of the coarsest level and $N = 2, 3$. Details of the coarse grid generation is given in Martynenko (2006).

6.3 Multigrid cycle

Multigrid cycles for simulation of flows with given and unspecified mass flow rates are shown on Figure 15. There are two kinds of smoothing on the multigrid structure. One of them (marked as \circ) is intended for solving Σ -modified Navier–Stokes equations with computation of correction of the «multidimensional component of pressure». Another smoothing (marked as \blacksquare) is intended for computation of correction of the «one-dimensional component of

pressure» on the finest grid. In other words solution of the modified auxiliary problem is additional smoothing on the finest grid.

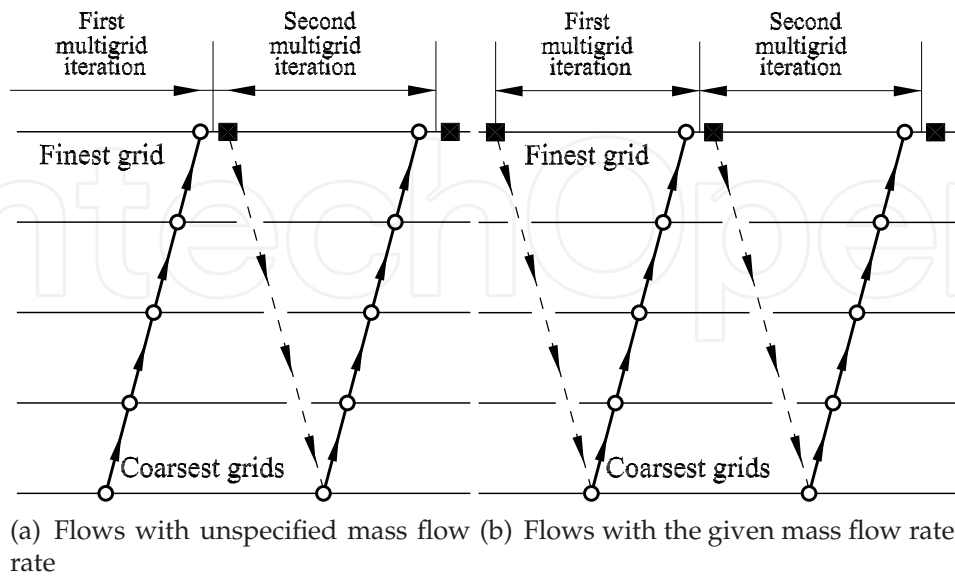


Fig. 15. Multigrid cycles

6.4 Numerical test

The algorithm is tested by simulation of unsteady flow in a driven cavity at $Re = 1000$. Law of the lid motion is taken as

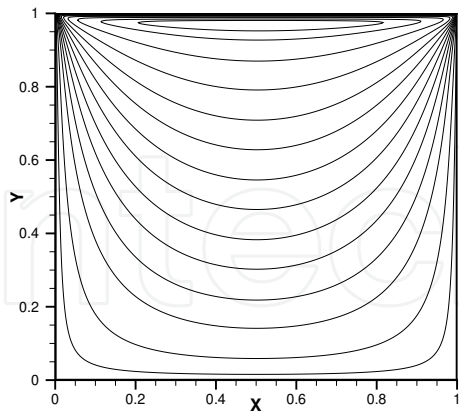
$$U_w^{(n)} = \min\left(\frac{n}{50}; 1\right),$$

and stopping criterion is posed as

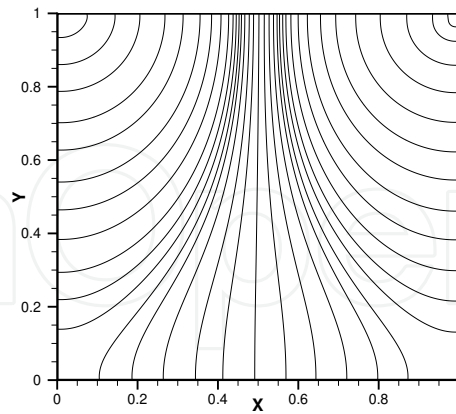
$$\max_{ij} \left| \frac{\partial u}{\partial x} + \frac{\partial v}{\partial y} \right|_{ij}^{(n+1)} < 10^{-10}.$$

Six-level multigrid structure with uniform finest staggered grid 501×501 ($h_t = h_x = h_y = 1/500$) is used for the test. Correction of the «multidimensional component of pressure» is computed using Uzawa algorithm with diagonal preconditioning.

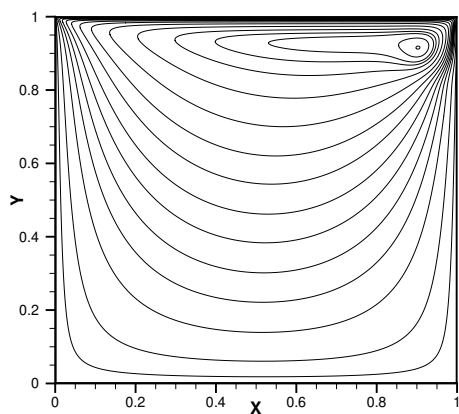
Figures 16–18 show evolution of the flow in the cavity. The main vortex is located near the lid after finish of the lid acceleration. Then the vortex moves to upper right corner under influence of the lid motion. After that the vortex moves along diagonal of the cavity to the center (Figure 16). Motion of the main vortex generates two additional vortices (Figure 17). The first vortex is formed in the lower corner, but the second vortex is formed on right vertical wall of the cavity. Location of the corner vortex is stable because of its motion is limited by the cavity walls. However the wall vortex can moving under influence of the main vortex. Corner and wall vortices agglomerate in common vortex. Agglomerated vortex tends to stable corner position, but a new corner vortex is generated in the left lower corner of the cavity. Figure 18 represents close-to-steady flow picture in the cavity.



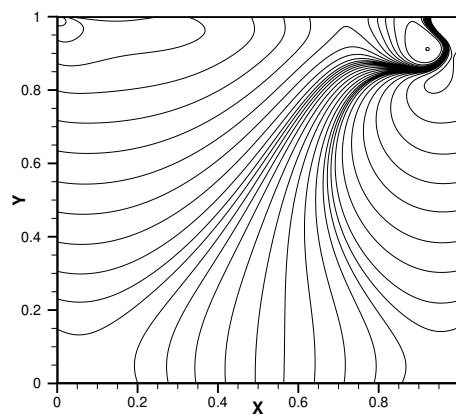
(a) Isolines of stream function ($n = 50$)



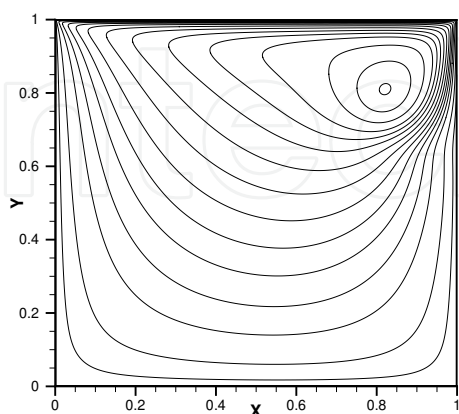
(b) Isobars ($n = 50$)



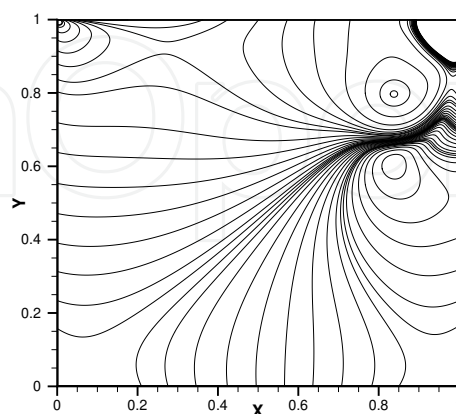
(c) Isolines of stream function ($n = 400$)



(d) Isobars ($n = 400$)

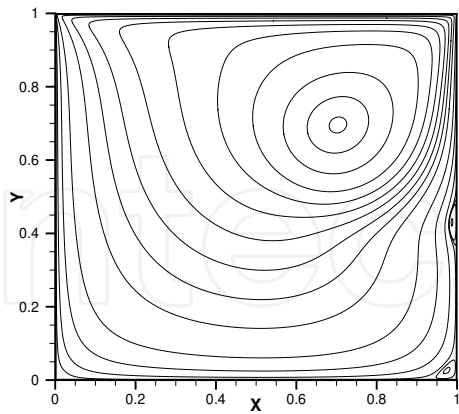
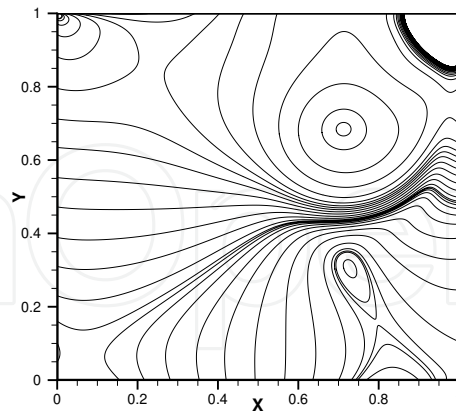
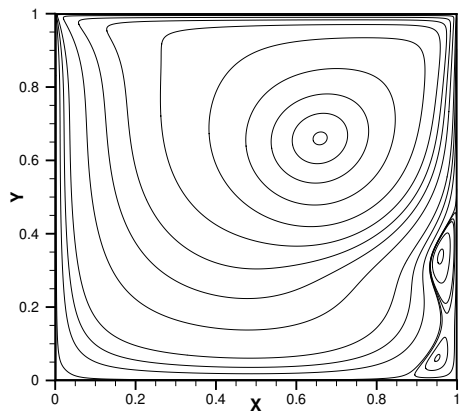
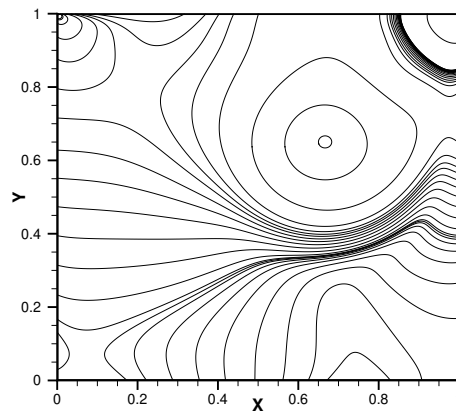
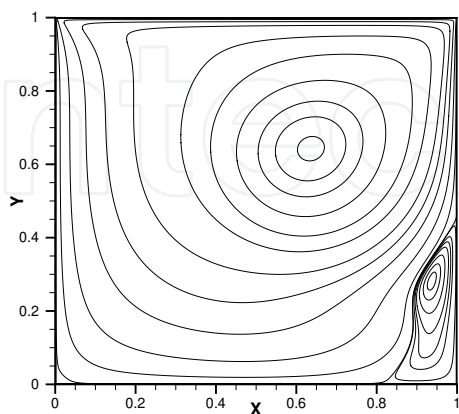
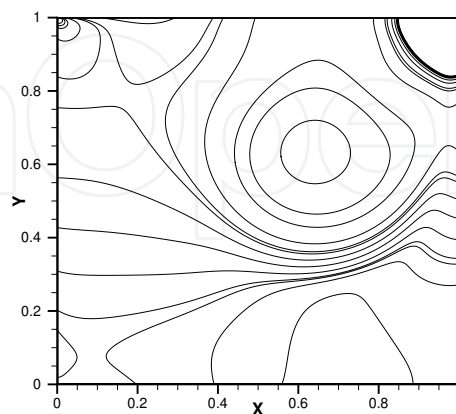


(e) Isolines of stream function ($n = 1000$)



(f) Isobars ($n = 1000$)

Fig. 16. Flow picture in the driven cavity ($n = 50, 400, 1000$)

(a) Isolines of stream function ($n = 2250$)(b) Isobars ($n = 2250$)(c) Isolines of stream function ($n = 3000$)(d) Isobars ($n = 3000$)(e) Isolines of stream function ($n = 3500$)(f) Isobars ($n = 3500$)Fig. 17. Flow picture in the driven cavity ($n = 2250, 3000, 3500$)

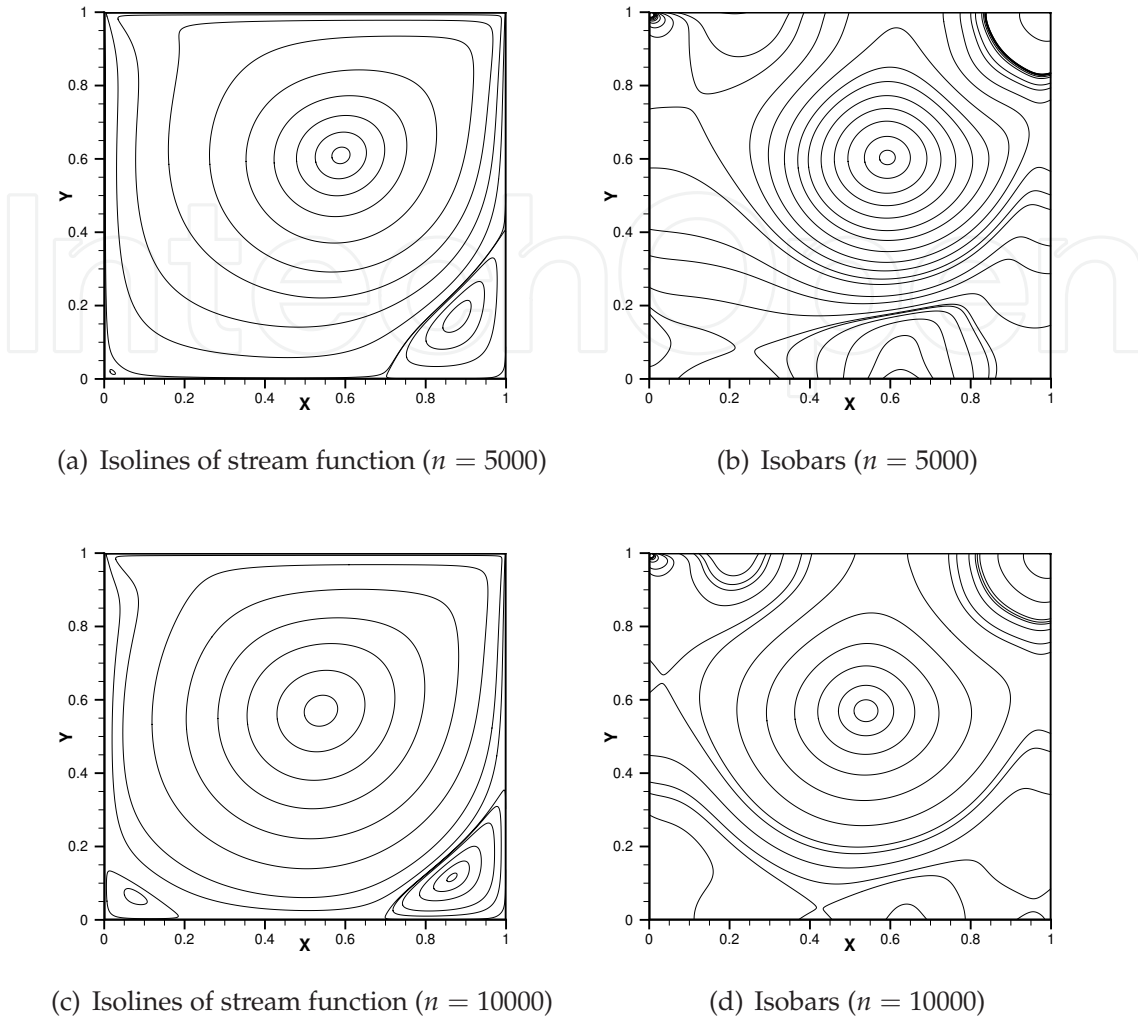


Fig. 18. Flow picture in the driven cavity ($n = 5000, 10000$)

7. Acknowledgements

Work supported by Russian Foundation for the Basic Research (project no. 09-01-00151). I wish to express a great appreciation to professor M.P. Galanin (Keldysh Institute of Applied Mathematics of Russian Academy of Sciences), who have guided and supported the researches.

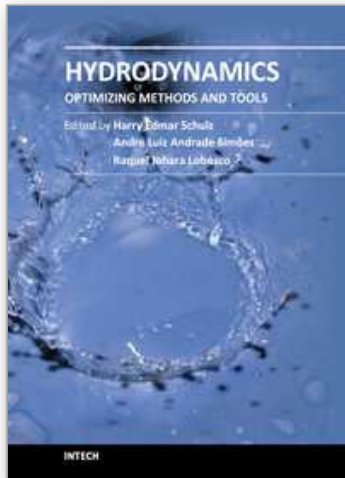
8. Conclusion

«Part of pressure» (i.e. sum of the «one-dimensional components» in decomposition (10)) can be computed using the simplified (pressure-unlinked) Navier–Stokes equations in primitive variables formulation and the mass conservation equations. «One-dimensional components of pressure» and corresponding velocity components are computed only in coupled manner. As a result, there are not pure segregated algorithms and pure density-based approach on structured grids. Proposed method does not require preconditioners and relaxation

parameters. Pressure decomposition is very efficient acceleration technique for simulation of directed fluid flows.

9. References

- Barton I.E. (1997) The entrance effect of laminar flow over a backward-facing step geometry, *Int. J. for Num. Meth. in Fluids*, Vol. 25, pp. 633-644.
- Benzi, M.; Golub, G.H.; Liesen, J. (2006) Numerical solution of saddle point problems, *Acta Numerica*, pp. 1-137.
- Briley, W.R. (1974) Numerical method for predicting three-dimensional steady viscous flow in ducts, *J. Comp. Phys.*, Vol. 14, pp.8-28.
- Gartling D. (1990) A test problem for outflow boundary conditions-flow over a backward-facing step, *Int. J. for Num. Meth. in Fluids*, Vol. 11, pp. 953-967.
- Ghia, U.; Ghia, K.N.; Shin, C.T. (1982) High-Re solutions for incompressible flow using the Navier-Stokes equations and a multigrid method, *J. Comp. Phys.*, Vol. 48, pp.387-411.
- Gresho, P.M.; Gartling, D.K.; Torczynski, J.R.; Cliffe, K.A.; Winters, K.H.; Garratt, T.G.; Spence, A.; Goodrich, J.W. (1993) Is a steady viscous incompressible two-dimensional flow over a backward-facing step at $Re=800$ stable? *Int. J. for Num. Meth. in Fluids*, Vol. 17, pp. 501-541.
- Keskar, J.; Lin, D.A. (1999) Computation of laminar backward-facing step flow at $Re=800$ with a spectral domain decomposition method, *Int. J. for Num. Meth. in Fluids*, Vol. 29, pp. 411-427.
- Martynenko, S.I. (2006) Robust Multigrid Technique for black box software, *Comp. Meth. in Appl. Math.*, Vol. 6, No. 4, pp.413-435.
- Martynenko, S.I. (2009) A physical approach to development of numerical methods for solving Navier-Stokes equations in primitive variables formulation, *Int. J. of Comp. Science and Math.*, Vol. 2, No. 4, pp.291-307.
- Martynenko, S.I. (2010) Potentialities of the Robust Multigrid Technique, *Comp. Meth. in Appl. Math.*, Vol. 10, No. 1, pp.87-94.
- Vanka S.P. (1986) Block-implicit multigrid solution of Navier–Stokes equations in primitive variables, *J. Comp. Phys.*, Vol. 65, pp.138-158.
- Wesseling, P. (1991) *An Introduction to Multigrid Methods*, Wiley, Chichester.



Hydrodynamics - Optimizing Methods and Tools

Edited by Prof. Harry Schulz

ISBN 978-953-307-712-3

Hard cover, 420 pages

Publisher InTech

Published online 26, October, 2011

Published in print edition October, 2011

The constant evolution of the calculation capacity of the modern computers implies in a permanent effort to adjust the existing numerical codes, or to create new codes following new points of view, aiming to adequately simulate fluid flows and the related transport of physical properties. Additionally, the continuous improving of laboratory devices and equipment, which allow to record and measure fluid flows with a higher degree of details, induces to elaborate specific experiments, in order to shed light in unsolved aspects of the phenomena related to these flows. This volume presents conclusions about different aspects of calculated and observed flows, discussing the tools used in the analyses. It contains eighteen chapters, organized in four sections: 1) Smoothed Spheres, 2) Models and Codes in Fluid Dynamics, 3) Complex Hydraulic Engineering Applications, 4) Hydrodynamics and Heat/Mass Transfer. The chapters present results directed to the optimization of the methods and tools of Hydrodynamics.

How to reference

In order to correctly reference this scholarly work, feel free to copy and paste the following:

Sergey Martynenko (2011). Convergence Acceleration of Iterative Algorithms for Solving Navier–Stokes Equations on Structured Grids, Hydrodynamics - Optimizing Methods and Tools, Prof. Harry Schulz (Ed.), ISBN: 978-953-307-712-3, InTech, Available from: <http://www.intechopen.com/books/hydrodynamics-optimizing-methods-and-tools/convergence-acceleration-of-iterative-algorithms-for-solving-navier-stokes-equations-on-structured-g>

INTECH
open science | open minds

InTech Europe

University Campus STeP Ri
Slavka Krautzeka 83/A
51000 Rijeka, Croatia
Phone: +385 (51) 770 447
Fax: +385 (51) 686 166
www.intechopen.com

InTech China

Unit 405, Office Block, Hotel Equatorial Shanghai
No.65, Yan An Road (West), Shanghai, 200040, China
中国上海市延安西路65号上海国际贵都大饭店办公楼405单元
Phone: +86-21-62489820
Fax: +86-21-62489821

© 2011 The Author(s). Licensee IntechOpen. This is an open access article distributed under the terms of the [Creative Commons Attribution 3.0 License](#), which permits unrestricted use, distribution, and reproduction in any medium, provided the original work is properly cited.

IntechOpen

IntechOpen